RSC Advances

ROYAL SOCIETY OF CHEMISTRY

www.rsc.org/advances

Structural Characterization and Multiferroic Properties of Hexagonal Nano-sized $YMnO_3$ Developed by Low Temperature Precursor Route

Tokeer Ahmad*, Irfan H. Lone and Mohd Ubaidullah

Nanochemistry Laboratory, Department of Chemistry, Jamia Millia Islamia, New Delhi-110025, India.

*Corresponding Author Address:

E-mail: tahmad3@jmi.ac.in

Phone: 91-11-26981717, Extn: 3261

Fax: 91-11- 26980229

Abstract:

Multiferroic $YMnO_3$ nanoparticles with narrow size distribution and high specific surface area (304 m^2g^{-1}) were synthesized using low temperature polymeric citrate precursor route for the first time. The crystal structure of monophasic hexagonal $YMnO_3$ nanoparticles was estimated by powder X-ray diffraction studies. The transmission and scanning electron microscopic studies revealed nearly hexagonal nanostructures with an average grain size of ~ 48 nm. The optical band gap was found to be 3.7 eV and photoluminescence studies also suggest the wide band gap semiconducting nature of $YMnO_3$. DC-magnetization studies of $YMnO_3$ nanoparticles exhibit ferromagnetic hysteresis with saturation magnetization of 21 $emug^{-1}$. The appearance of room temperature ferroelectric loop at 50 kHz has been observed for the first time with an improved remanent polarization of 0.0084 $\mu C/cm^2$. The dielectric properties on sintered disks were also investigated as a function of frequency and temperature.

Key words: Nanoparticles, Multiferroics, Chemical synthesis, Surface area, Optical properties, Hysteresis.

Introduction:

Nanocrystalline multiferroic oxides have received remarkable interest of research in the past decade due to the coexistence of magnetically and ferroelectrically ordered states. The magnetoelectric phenomena arise from the coupling between the pairing of magnetic properties by an application of electric field and vice versa.[1–4] The study of multiferroic materials has became an interesting subject because of their possible applications in electric devices such as electric field induced magnetic memory effects and electro-optic transducer controlled by magnetic fields.[5–7] They have also been used in the field of radio, television, satellite communications, sensors, memory devices and digital recording media.[1, 3] Among them, $YMnO_3$ has shown wide range of applications in capacitors, transducers, actuators, nonvolatile information storages, spintronic devices and magnetoelectric sensors.[8-10]

Several chemical routes viz. reverse micelles,[11] solvothermal,[12] sonochemical[13] and polymeric citrate precursor[14] methods are available in literature for the fabrication of various nanostructures. Among them, Pechini type polymeric precursor method[15] is highly efficient to prepare homogeneous nanostructures without careful control of gel processing time. Nanocrystalline $YMnO_3$ has been prepared by hydrothermal[16] and sol-gel[17-19] methods. However, there is no report in literature for the synthesis of $YMnO_3$ nanoparticles using polymeric citrate precursor method to the best of our knowledge. The crystal structure of nanoscale hexagonal $YMnO_3$ deviates from the bulk and the ferroelectric displacement of Y3+ cations decays progressively with the decreasing size as well as different magnetic interactions with different grain sizes were also reported.[20] Such diverse properties have not been investigated to large extent and the origin of these properties of $YMnO_3$ is still ambiguous. The phase selective synthesis of nano-sized $YMnO_3$ at low temperature is found to be difficult, because most of the meta stable phases are generally stabilized at high temperature and pressure. The effect of nanosize on magnetic properties like curie

temperature of $MnFe_2O_4$ system as compared to bulk was due to finite size scaling. A proposed explanation for the anomalous behavior of $MnFe_2O_4$ prepared by wet and standard ceramic methods was due to non-equilibrium cation size distribution over tetrahedral and octahedral sublattices.[21-23] This mechanism is not been reported for $YMnO_3$.

In this paper, we report the synthesis of $YMnO_3$ nanoparticles by metal organic precursor method using citric acid and ethylene glycol as complexing agents for the first time. As prepared nanoparticles were then investigated by means of X-ray diffraction (XRD), scanning electron microscopy (SEM), transmission electron microscopy (TEM), UV-visible, fluorescence and BET surface area studies. The electrical and magnetic properties have been studied in detail for the multiferroic characterization.

2. Experimental:

The following chemicals were used in the synthesis: yttrium nitrate (Alfa Aesar; 99.9%), manganese acetate (Spectrochem; 99%), ethylene glycol (SD fine-chem Ltd; 99%) and citric acid (Spectrochem; 99%). All the chemicals were of analytical grade and used as received without further purification.

1.4 ml of ethylene glycol (EG) was taken in a 400 ml beaker and 25 ml of 0.1 M aqueous solution of manganese acetate was added under constant stirring. The mixture was stirred for about 10-15 minutes to obtain a clear transparent solution, followed by the addition of 21.0135g of dried citric acid (CA), so that the molar ratios of ethylene glycol: citric acid: manganese ion were fixed at 10:40:1. The contents were allowed on continuous stirring at room temperature for about 2 hours to obtain clear solution of the precursor. After complete dissolution, 25 ml of 0.1M of aqueous solution of yttrium nitrate was added to this solution and stirred for another 2 hours. The clear solution thus prepared, was heated at 70^{o}C for 2 hours to remove excess water and to accelerate the polyesterification reaction between CA

and EG. The solution became viscous which was then placed in muffle furnace at 135^{o}C for 20 hours to evaporate the solvent and appearance of semi-solid mass has been observed during the course of the polymerization. The semisolid mass was then charred at 300^{o}C for 2 hours in a muffle furnace to produce a black mass product. The charred sample was lightly ground to a fine powder using a Teflon rod. This ground black mass is referred to as precursor. The precursor was further heated at 800^{o}C in static air for 12 hours in a microprocessor controlled high temperature furnace to obtain $YMnO_3$ nanoparticles. The flow chart depicting the various steps involved in the synthesis of $YMnO_3$ nanoparticles is shown in fig.1.

3. Instrumentation:

Powder X-ray diffraction studies have been carried out on Bruker D8 Advance X-ray diffractometer using Ni-filtered Cu-Kα radiation of wavelength λ = 1.54056 Å. The diffraction pattern was recorded in the 2θ range of 10^{o} to 70^{o} with the step size of 0.05^{o} and step time of 1 second. The Kα2 reflections were removed by the normal stripping procedure. The crystallite size of $YMnO_3$ powder was determined by the X-ray line broadening studies on (112) crystal plane using Scherrer's equation[24] $d = k\lambda/\beta\cos\theta$, where d is the average diameter of the grains, k is a particle shape factor and taken as 0.9 for spherical nanoparticles, λ is the wavelength of X-rays, θ is the corresponding Bragg angle and β is the full width at half maximum (FWHM) and can be calculated by using the Warren's formula,[25] i.e. $\beta^2 = \beta_M^2 - \beta_S^2$, where β_M and β_S are the full width at half maximum of sample and standard respectively.

Transmission electron microscopic (TEM) studies have been carried out by using FEI Technai G^2 20 transmission electron microscope with an accelerating voltage of 200 kV. TEM specimens were prepared by taking a small amount of the finely ground powder, which was then dispersed in absolute ethanol and sonicated for about 30 minutes with the help of

ultrasonicator (Model: UP-500 Ultrasonic Processor). A drop from the micropipette (about 100μL volume) of the dispersed sample was placed on a copper grid coated with carbon film. Scanning electron microscopic (SEM) studies were carried out on ZEISS EVO 50 SEM operated at 30 kV acceleration voltage which provides a resolution of 5 nm. The surface area of the sample was recorded at liquid nitrogen temperature (77 K) using BET surface area analyser (Model: Nova 2000e, Quantachrome Instruments Limited, USA), by using 'Multipoint BET Method'. Approximately 0.08g of the powder sample was placed in the sample cell and allowed to degas at one of the degassing stations for 3 hours at 250^{o}C in a vacuum degassing mode. This removes the contamination of water vapour and adsorbed gases from the sample. The degassed sample was then subjected for the analysis and the data was recorded by admitting known quantities of adsorbing nitrogen gas into the sample cell containing the solid for adsorption. As the adsorption occurs, the pressure in the cell changes until equilibrium is reached. From the BET plot, the specific surface area is calculated using the multipoint BET equation. The powder samples of $YMnO_3$ nanoparticles were dissolved in ethanol (Merck) and the band gap was determined from the optical absorption spectra obtained using a Perkin-Elmer double-beam Lamda-35 spectrophotometer. Pure ethanol was used as the reference blank solution for the sample. Fluorescence spectra were obtained using a Perkin-Elmer LS-55 spectrofluorophotometer after dissolving the powders in ethanol.

For dielectric and ferroelectric studies, a pellet of $YMnO_3$ nanoparticles (diameter = 8 mm) was prepared at a pressure of 5 tons by using 5% PVA solution as binding agent. The pellet was then sintered under static air at 1000^{o}C for 8 hrs. Colloidal silver paint (Ted Pella, Inc.) was coated on both the surface of pellet and dry in oven. Dielectric measurements were carried out using HF-LCR meter (6505P, Wayne Kerr electronics, UK) in the frequency range of 100 kHz–2 MHz over a temperature range of 30–430^{o}C. The principle of parallel plate capacitor was employed for the evaluation of permittivity. The data acquisition was

automated by interfacing the LCR meter with a virtual instrumentation package called LABVIEW (National Instruments). The dielectric permittivity of the sample was calculated using the relation; $C = \varepsilon_o \varepsilon_r A/d$, where C is the capacitance of the parallel plate capacitor, d is the thickness and A is the area of cross section, ε_0 is the permittivity of free space and ε_r is the relative permittivity of the dielectric material. Further, on these sintered pellets, the room temperature ferroelectric studies were carried out at 50 kHz frequency at different applied voltage by using the P-E loop tracer (M/s Radiant Instruments, USA). The magnetization studies were performed using the magnetic property measurement system (MPMS) SQUID magnetometer under an external magnetic field of ±60 kOe at temperatures ranging from 5 to 300 K.

4. Results and discussion:

Powder X-ray diffraction pattern of monophasic $YMnO_3$ is shown in fig. 2. All reflections could be indexed to the primitive hexagonal $YMnO_3$ (JCPDS 25-1079). The X-ray line broadening studies using Scherrer's formula have been carried out on (112) crystal plane and crystallite size was found to be 52 nm. To investigate the surface texture, particle size, morphology and crystallinity of $YMnO_3$, TEM, SEM and SAED investigations were carried out. The TEM, SEM and SAED images of the sample calcined at 800^{o}C suggest that the particles are nanocrystalline of nearly hexagonal shape with an average grain size of ~ 48 nm as shown in fig. 3 (a, b and c). The agglomeration in $YMnO_3$ nanoparticles could be seen due to the synthesis temperature which may attributes to the grain diffusion. The studies showed that the X-ray size is well supported with the TEM size studies.

The Brunauer-Emmett-Teller (BET) gas adsorption method has become the most widely used standard procedure for the determination of the surface area of finely divided and porous materials. The specific surface area of $YMnO_3$ nanoparticles was determined using the multipoint BET method and it was found to be 304 m^2g^{-1} as shown in fig. 4 (a). The

observed surface area was found to be comparatively much higher than the earlier reports[26]. The nitrogen adsorption-desorption isotherm of $YMnO_3$ nanoparticles is presented in fig. 4(b). The prominent attributed hysteresis loop of the adsorption isotherms could be ascribed to the type-IV isotherm which can be normally associated with capillary condensation in mesopores[27]. The BJH pore size distribution curve (fig. 5a) confirmed the predominance of mesopore of diameters 15 Å to 25 Å of $YMnO_3$ nanoparticles. However DA plot which displayed average pore radius of 15 Å is shown in fig. 5b. The positive BET constant c value obtained from BET plot of $YMnO_3$ was found to be high (3.55) which is associated to the high affinity and high heat of adsorption of $YMnO_3$ with the adsorbate gas (N_2). The average particle size of the nanoparticles could also be calculated by using the equation, $D_{BET} = 6000/\rho S_w$ where the symbol D_{BET}, ρ and S_w stands for average diameter (nm) of the spherical particle, theoretical density (gcm^{-3}) and specific surface area (m^2g^{-1}) of the sample respectively.[28, 29] The particle size using BET surface area studies comes out to be 2.91 nm. This value is much smaller than the measured values, which indicates that the surfaces of $YMnO_3$ nanoparticles are multidimensional and not smooth.

The optical absorption spectrum of $YMnO_3$ nanoparticles is presented in fig. 6a. The optical absorption spectra reveal that $YMnO_3$ shows semiconductor-like absorption. The band gap energy of as-prepared nanoparticles is calculated using the following equation[30, 31]; $\alpha h\nu = A(h\nu - E_g)^2$, where α, v, A, and E_g are the absorption coefficient, light frequency, proportionality constant, and band gap energy, respectively. The band gap of the $YMnO_3$ nanoparticles is calculated from the extrapolation of the linear portion of the plot of $\alpha h\nu^2$ vs $h\nu$ graph to the abscissa (inset in fig.6a) and was found to be 3.7 eV. In nanomaterials, the band gap gets widen, because the number of overlapping orbitals or energy levels decreases as compared to bulk phase of same material[32] and hence in the present case, the band gap is larger as compared to earlier value of 1.5 and 2 eV.[33] A little

attention is given on the photoluminescence (PL) study of $YMnO_3$ nanoparticles. Fig. 6b shows the PL spectra of $YMnO_3$ nanoparticles at two different excitation wavelengths and the observed emission peaks appeared at 336 and 350 nm respectively and this indicates that as-prepared nanoparticles are wide-band gap semiconductor.

The dielectric properties of $YMnO_3$ nanoparticles have been measured on sintered disk at 1000^oC by using HFLCR meter as a function of frequency and temperature as shown in fig. 7 (a and b). The dielectric constant and dielectric loss was found to decrease with frequency. The values of dielectric constant and dielectric loss were found to be 21.2 and 1.04 at 100 kHz and then decreases to the value of 14.1 and 0.67 at 1 MHz respectively (fig. 7a). This effect of dielectric characteristics with frequency was earlier explained on the basis of Maxwell–Wagner interfacial polarization.[34] The temperature dependence of the dielectric properties of $YMnO_3$ nanoparticles at 100 kHz frequency was studied in the temperature range of 30^oC to 430^oC as shown in fig. 7b. Both the dielectric constant and dielectric loss were found stable till 250^oC temperature and thereafter increases with the increase in temperature.

Polarization–electric fields (P–E) hysteresis studies of $YMnO_3$ nanoparticles have been carried out in the applied electric field range of 100 to 400 V at 50 kHz frequency as shown in fig. 8. The area of the P-E loop decreases with the decrease of applied voltage and achieved relatively better remanent polarization (P_r) of 0.0084 $\mu C/cm^2$, saturation polarization (P_s) of 0.011$\mu C/cm^2$ and coercive field (E_c) of 1.23 kV/cm at an applied field of 400 V. The ferroelectric ordering of $YMnO_3$ was earlier observed at 21 K, however this is the first report on room temperature ferroelectricity in $YMnO_3$ nanoparticles to the best of our knowledge.[35] Ferroelectricity may be associated to the buckling of the layered MnO_5 polyhedral, accompanied by displacement of the Y^{3+} ions, which lead to a net electric polarization. The polarization is a consequence of the unusual Y-site coordination and the

triangular and layered MnO_5 network.[36] This type of mechanism can also be applied in $YMnO_3$ nanoparticles as it was earlier observed in bulk as well as thin films of $YMnO_3$. Although the mechanism of ferroelectricity of $YMnO_3$ were given by the displacement Y cation, expressed by the buckling parameter and the size dependent positions indicate a reduction of the MnO_5 bipyramidal tilting. But no one has reported the room temperature ferroelectric loop in $YMnO_3$ nanoparticles.

The investigation of the magnetic properties of as-prepared $YMnO_3$ nanoparticles has been carried out on MPMS SQUID magnetometer under an external magnetic field of ±60 kOe in the temperature range of 5 to 300 K. The molar magnetic susceptibility of $YMnO_3$ nanoparticles were measured as a function of temperature at 1 kOe as shown in fig.9a. The molar susceptibility (χ_M) decreases rapidly with increasing temperature till 50 K, beyond which a slight decrease was observed which may be associated with the ferromagnetic ordering in $YMnO_3$ nanoparticles with Curie temperature of 50 K. The temperature (T) dependence of inverse susceptibility (χ^{-1}) was also fitted as shown in fig. 9a, which implies the weak ferromagnetic interaction and it may be due to the nanocrystalline nature of the material.[37] Fig. 9b is the M-H plot of $YMnO_3$ nanoparticles at 5K which confirms the appearance of ferromagnetic hysteresis loop with the saturation magnetization of 21.19 emu g^{-1}, remanent magnetization of 0.95 emu g^{-1} and coercive field of -980 kOe. The results of ferromagnetism were found better as compared to earlier report.[38] M-H data collected earlier shows that the antiferromagnetic interaction increases by the increase of particle size and there were narrow hysteresis loop for 20 nm sized $YMnO_3$, indicating weak ferromagnetic interactions. However, it was not observed for large crystallites (170 nm) and shown excellent agreement with reported values for bulk $YMnO_3$.[20, 39] Hence, the largest crystallites display similar magnetic properties to the bulk material. Thus, these results show weak ferromagnetic interactions in as-prepared $YMnO_3$ nanoparticles due to small particle size (48

nm) which was further supported by the narrow hysteresis loop. Thus, the appearance of ferroelectric as well as ferromagnetic hysteresis in $YMnO_3$ nanoparticles attributes to the multiferroic characteristics in the as-prepared material.

Conclusions:

$YMnO_3$ nanoparticles with an average grain size of 48 nm were synthesized by a simple soft chemical route using citric acid as the chelating agent. XRD, SEM, TEM, SAED and BET surface area techniques were used to confirm the phase purity, morphology, crystalline nature and size distribution of the nanoparticles. The optical properties show that the value of band gap of $YMnO_3$ nanoparticles lies in the semiconducting range and also possesses the photoluminescent property. Existence of ferroelectricity along with ferromagnetism in $YMnO_3$ nanoparticles confirms the multiferroic characteristics of the material.

Acknowledgements

This work is financially supported by Innovative Research Activities of Jamia Millia Islamia, New Delhi (AC-6(15)/RO/2014). Authors thank IIT-Delhi for XRD analysis, AIIMS New Delhi for electron microscopic studies and Prof. K. V. Ramanujachary (Rowan University, USA) for carrying out the magnetic measurements. We gratefully acknowledge Dr. V. R. Reddy (UGC-DAE Indore) for P-E measurements and valuable discussions. IHL specially thanks to University Grant commission (UGC) New Delhi for JRF and SRF fellowships.

References:

[1] S. W. Cheong and M. Mostovoy, *Nature Mater.* 2007, **6**, 13-20.

[2] N. Fujimura, T. Ishida, T. Yoshimura and T. Ito, *Appl. Phys. Lett.* 1996, **69**, 1011.

[3] R. Ramesh and N. A. Spaldin, *Nature Mater.* 2007, **6**, 21.

[4] P. A. Sharma, J. S. Ahn, N. Hur, S. Park, S. B. Kim, S. Lee, J. G. Park, S. Guha and S. W. Cheong, *Phys. Rev. Lett.* 2004, **93**, 177202.

[5] N. Hur, S. Park, A. P. Sharma, A. J. Ahn, S. Guha, W. S. Cheong, *Nature*, 2004, **429**, 392–395.

[6] M. W. Zhu and G. Z. Ye, *Ceram. Int.* 2004, **30**, 1435–1442.

[7] R. Seshadri and A. N. Hill, *Chem. Mater.* 2001, **13**, 2892–2899.

[8] O. Auciello, J. F. Scott and R. Ramesh, *Phys. Today*, 1998, **51,** 22–27.

[9] I. J. Busch-Vishniac, *Phys. Today,* 1998, **51,** 28–34.

[10] J. Wang, M. Y. Li, X. L. Liu, L. Pei, J. Liu, B. F. Yu and X. Z. Zhao, *Chin. Phys. Lett.* 2009, **26**, 117301.

[11] A. K. Ganguli, S. Vaidya and T. Ahmad, *Bull. Mater. Sci.* 2008, **31(3)**, 415-419.

[12] T. Ahmad, S. Khatoon, K. Coolahan and S. E. Lofland, *J. Mater. Res.* 2013, **28**, 1245-1253.

[13] I. A. Wani and T. Ahmad, *Colloid Surf. B* 2013, **101**, 162-170.

[14] T. Ahmad, I. H. Lone, M. Ubaidullah and K. Coolhan, *Mater. Res. Bull*. 2013, **48**, 4723-4728.

[15] M. P. Pechini, US Pat., 330697, 1967.

[16] R. D. Kumar and R. Jayavel, *Mater. Lett.* 2013, **113**, 210-213.

[17] B. Raneesh, A. Saha and N. Kalarikkal, *Radiat. Phys. Chem.* 2013, **89**, 28-32.

[18] A. Han, M. Zhao, M. Ye, J. Liao, Z. Zhang and N. Li, *Sol. Energy,* 2013, **91**, 32-36.

[19] K. Tadanaga, H. Kitahata, T. Minami, N. Fujimura and T. Ito, *J. Sol-Gel Sci. Technol.*

1998, **13**, 903-908.

[20] K. Bergum, H. Okamoto, H. Fjellvag, T. Grande, M-A. Einarsruda, and S. M. Selbach, *Dalton Trans.,* 2011, **40**, 7583-7589.

[21] P. J. van der Zaag, A. Noordermeer, M. T. Johnson and P. F. Bongers, *Phys. Rev. Lett*., 1992, **68**, 3112.

[22] P. J. van der Zaag, V. A. M. Brabers, M. T. Johnson, A. Noordermeer and P. F. Bongers, *Phys. Rev. B,* 1995, **51**, 12009-12010.

[23] C. N. Chinnasamy,A. Yang, S. D. Yoon, K. Hsu , M. D. Shultz, E. E. Carpenter, S. Mukerjee, C. Vittoria and V. G. Harris, *J. Appl. Phys.* 2007, **101**, 09M509 (1-3).

[24] L. S. Birks and H. Friedman, *J. Appl. Phys.* 1946, **17**, 687.

[25] B. E. Warren and B. L. Averbach, *J. Appl. Phys.,* 1952, **23**, 497.

[26] T. Hyodo, M. Kayashi, N. Miura and N. Yamazoe, *J. Electrochem. Soc.* 1996, **143**, 266-267.

[27] S. Brunauer and D. Teller, *J. Am. Chem. Soc.* 1940, **62,** 1723.

[28] I. A. Wani, S. Khatoon, A. Ganguly, J. Ahmed, A. K. Ganguli and T. Ahmad, *Mater. Res. Bull.* 2010, **45**, 1033-1038.

[29] J.G. Li, T. Ikegami, Y. Wang and T. Mori, *J. Am. Ceram. Soc*. 2003, **86,** 915–921.

[30] J. I. Pancove, Englewood Cliffs, NJ: Prentice Hall, 1971.

[31] J. Tauc, R. Grigorovici and A. Vancu, *Phys. Status Solid,* 1966**, 15**, 627–637.

[32] A. P. Alivisatos, *Science*, 1996, **27**, 933-937.

[33] A. M. Kalashnikova and R. V. Pisarev, *JETP Letters,* 2003, **78**, 143.

[34] K. W. Wagner, *Ann. Phys.* 1993, **40,** 818.

[35] S. Ishiwata, Y. Tokunaga, Y. Taguchi and Y. Tokura, *J. Am. Chem. Soc.* 2011, **133**, 13818.

[36] B. B. van Aken, T. T. M. Palstra, A. Filippetti and N. A. Spaldin, *Nature Mater*. 2004, **3**, 164-170.

[37] C. Zhang, J. Su, X. Wang, F. Huang, J. Zhang, Y. Liu, L. Zhang, K. Min, Z. Wang, X. M. Lu and F. Yan, *J. Alloys Compd.* 2011, **509**, 7738–7741.

[38] R. D. Kumar and R. Jayavel, *Adv. Mater. Res.* 2012, **584**, 253-257.

[39] A. Munoz, J. A. Alonso, M. J. Martinez-Lope, M. T. Casais, J. L. Martinez and M. T. Fernandez-Diaz, *Phys. Rev. B*, 2000, **62**, 9498.

Figure Captions:

FIG.1. Flow chart for the synthesis of $YMnO_3$ nanoparticles using citrate precursor route.

FIG.2. Powder X-ray diffraction pattern of as-prepared $YMnO_3$ nanoparticles.

FIG. 3. (a) TEM, (b) SEM and (c) SAED images of $YMnO_3$ nanoparticles at 800^oC.

FIG.4. (a) BET plot and (b) nitrogen adsorption isotherm of $YMnO_3$ nanoparticles.

FIG. 5. (a) BJH and (b) DA pore size distribution plots of as-prepared $YMnO_3$ nanoparticles.

FIG. 6. (a) Optical absorbance and (b) photoluminescence spectra of $YMnO_3$ nanoparticles. Inset is the band gap energy determination plot.

FIG 7. Variation of dielectric constant and dielectric loss of $YMnO_3$ nanoparticles as a function of (a) frequency and (b) temperature.

FIG.8. P-E hysteresis studies of $YMnO_3$ nanoparticles at various electric fields.

FIG.9. (a) Temperature dependence of molar susceptibility at 1 kOe (b) M-H curve of $YMnO_3$ nanoparticles.

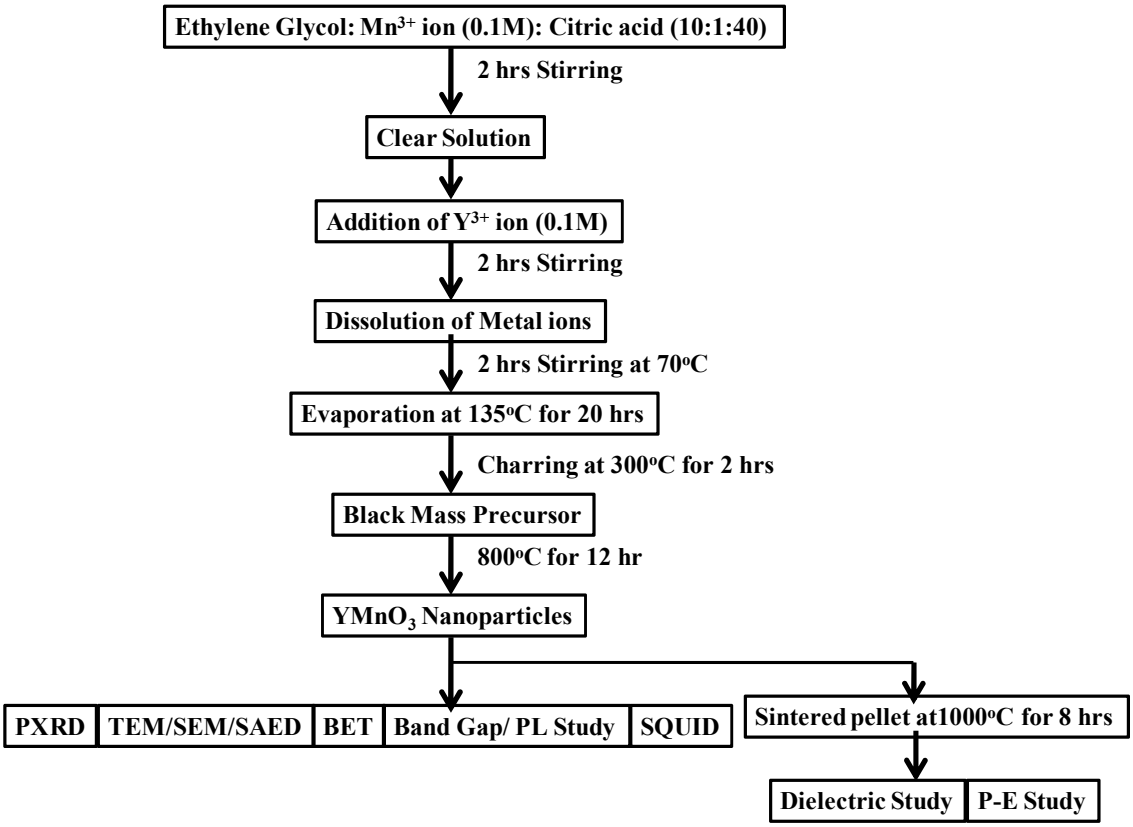

FIG.1

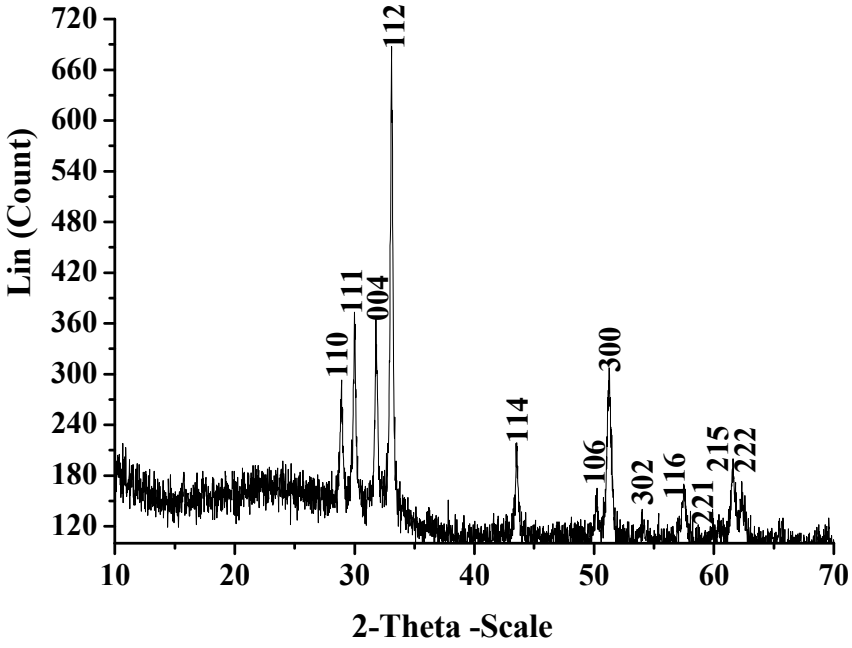

FIG.2

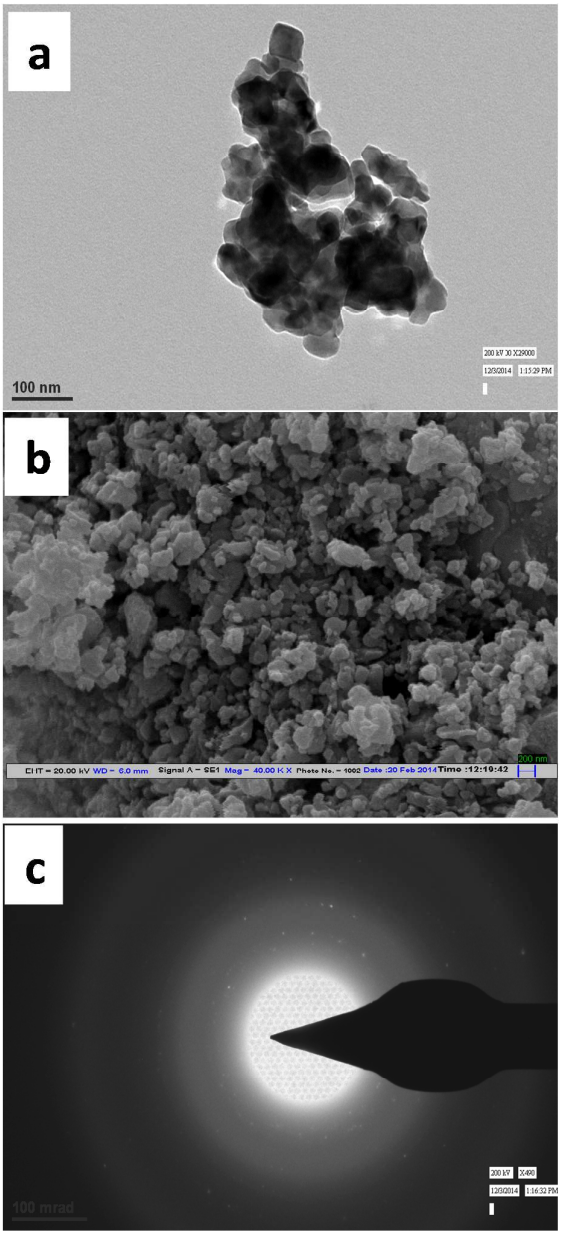

FIG.3

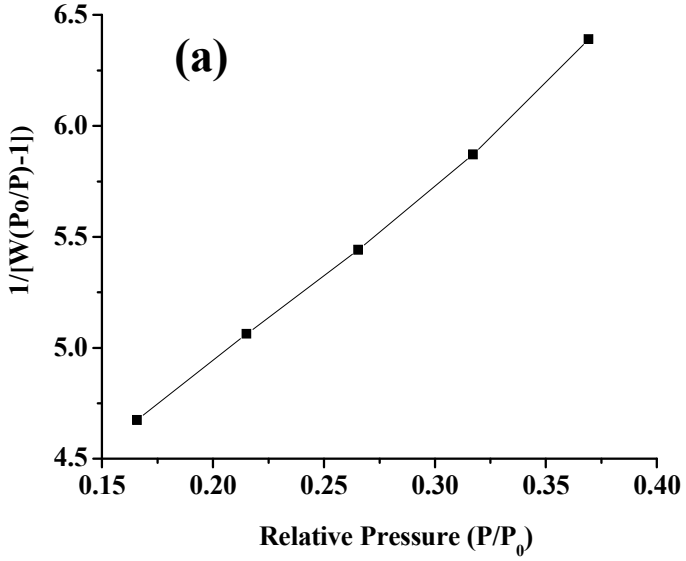

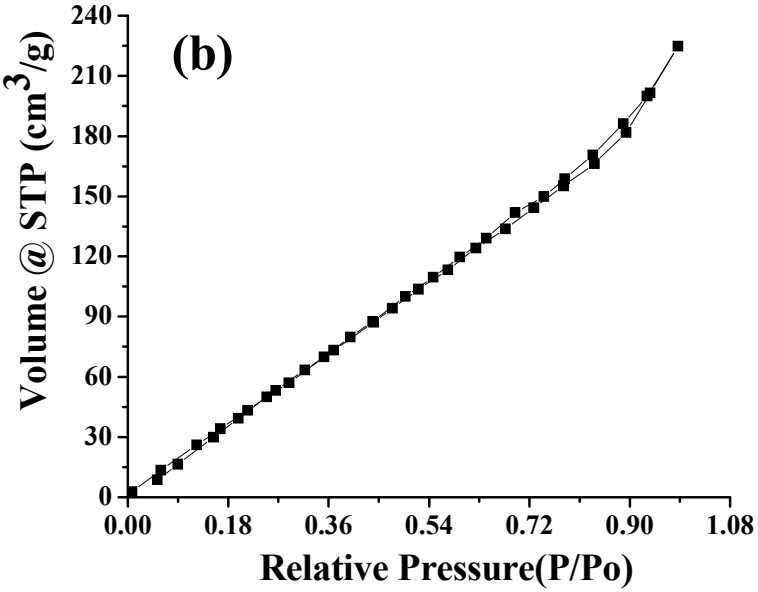

FIG. 4

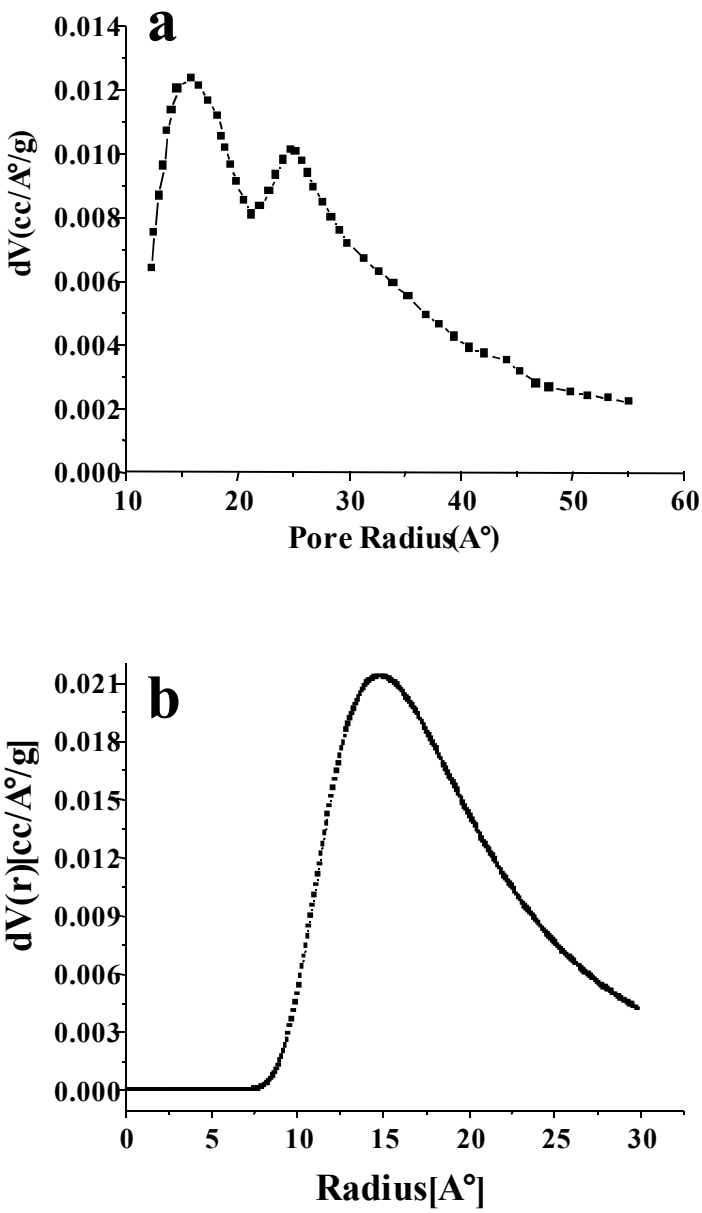

FIG. 5

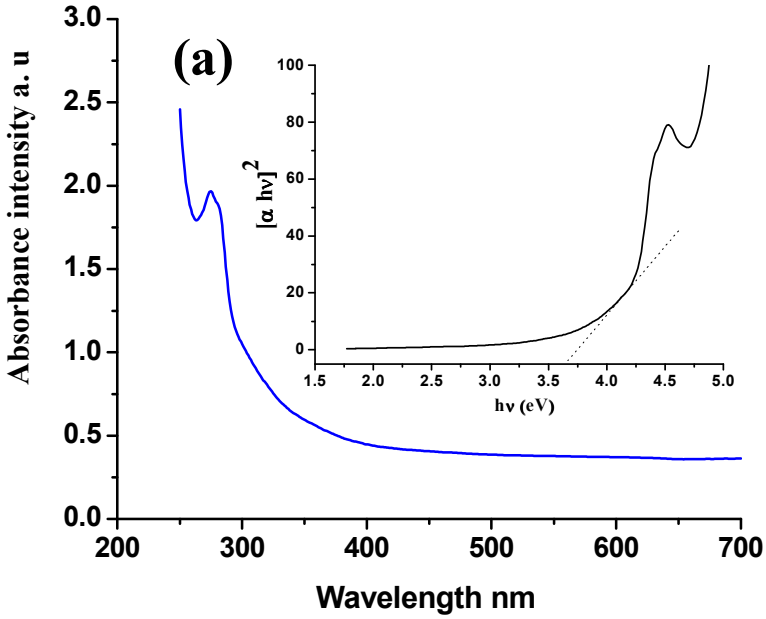

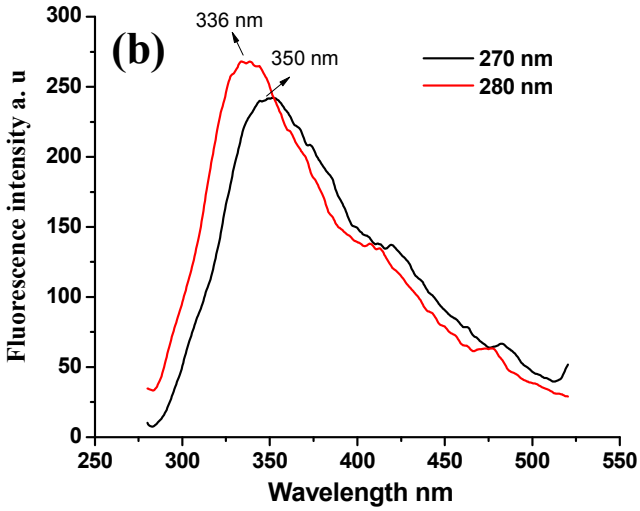

FIG.6

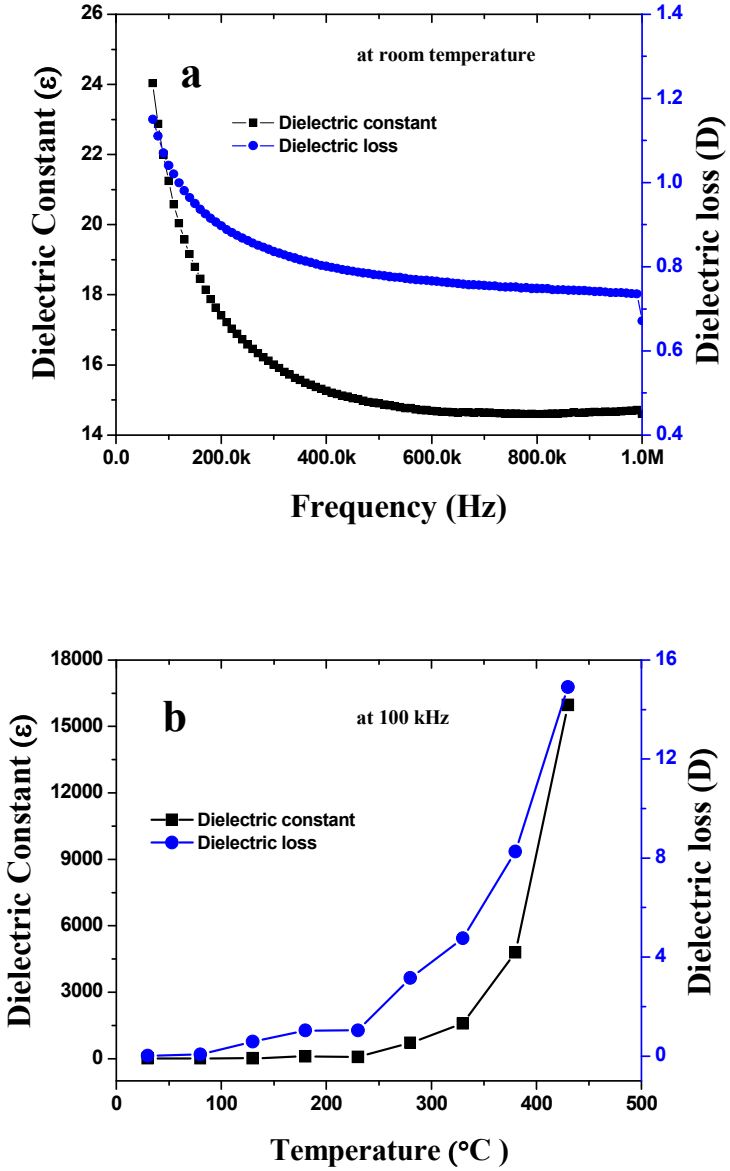

FIG. 7

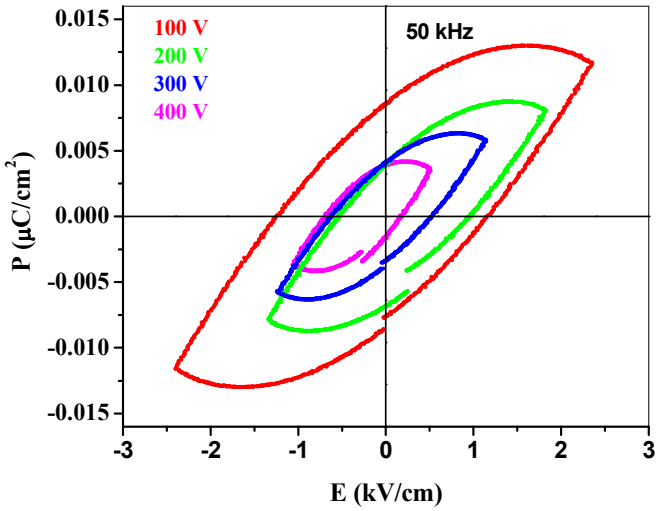

FIG. 8

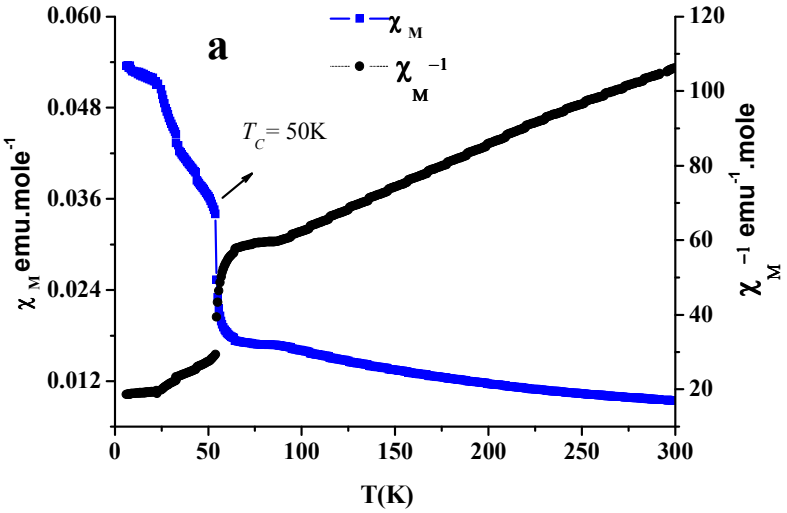

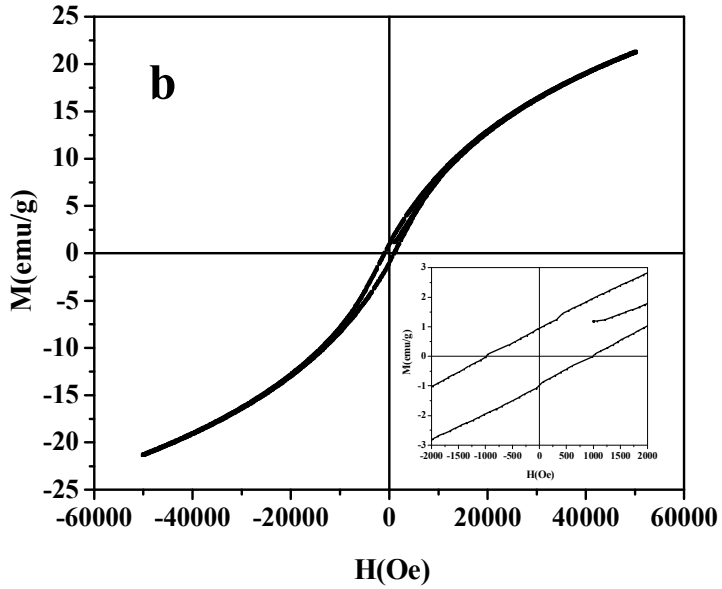

FIG. 9